A New Methodology for Two-Dimensional Numerical Simulation of Semiconductor Devices

Shan-Ping Chin, *Student Member, IEEE*, and Ching-Yuan Wu, *Member, IEEE*

***Abstract*—A new methodology for obtaining the self-consistent solution of semiconductor device equations discretized in the finite-difference scheme is proposed, in which a new discretized Green's function solution method is used to solve the two-dimensional discretized Poisson's equation and a surface mapping technique is developed to treat arbitrary surface boundary conditions. As a result of the proposed new solution method, the two-dimensional potential distribution can be expressed in terms of charge density distribution and bias conditions. Using the derived potential distribution, the SLOR-nonlinear iteration for the current continuity equations of both carriers can be performed by incorporating with a new algorithm to get the self-consistent solution of full set of semiconductor device equations without any outer iteration. Comparisons between the proposed method and the Gummel's method in Si-MESFET simulation are made. It is demonstrated that the convergent rate of the proposed method can be speeded up to 4–8 times over the Gummel's method. The proposed new iterative method can be incorporated with the conventional solution method such as the Gummel's method to get a stable and efficient computation scheme for device simulation.**

I. Introduction

THE electrical characteristics of the scaled semiconductor devices are sensitive to the device structure and the operational condition due to the multidimensional effects [1]. In general, fundamental device modeling may provide some valuable information for understanding the physics of semiconductor devices. However, an accurate analytical model becomes difficult to develop because of the complexity of mathematical treatment for the multidimensional effects and cannot be generalized for any device structure. Therefore, the device numerical simulation [2]–[5] based on the self-consistent calculation of semiconductor device equations has become important in device modeling.

In general, numerical techniques [6]–[8], [10] have become a standard method to solve semiconductor device equations. However, the primary problems concerning the two-dimensional numerical simulation are mainly due to the fact that a large nonlinear system must be solved iteratively to get the self-consistent solution of discretized semiconductor equations. Moreover, an efficient solution method becomes very difficult to develop for solving the full set of semiconductor device equations. The major reason is that the mutual coupling effect between the Poisson's equation and the current continuity equations is very strong. The convergent property becomes very poor when the decoupling method (the Gummel's method) is used, especially when the device is operated in the high-current level. The strongly nonlinear behavior of equations to be solved may produce significant error when the linear expansion is used. In general, this effect may cause the overshooting for the Newton's method if the initial condition of the numerical iteration is not in the contraction domain, and some physical quantities such as electron and hole densities may vary over a huge range, leading to arithmetic difficulties. For any device structure and bias conditions, no method can guarantee to be stable and efficient in solving the semiconductor equations. From this viewpoint, the development of a fundamental solution method for the semiconductor equations is necessary to enhance the flexibility in the selection of an iteration algorithm.

Recently, several new approaches [11], [12] have been developed by using the combination of the analytical method and the numerical techniques. In the Fourier-numerical method [11], all of the semiconductor equations are transformed into the discrete Fourier series by using the fast-Fourier transformation (FFT) method to get the well-conditioned matrix equations, and these matrices can be solved by the Newton's method to obtain the accurate result. On the other hand, the analytical solution of the 2-D Poisson's equation using the Green's function technique is used to obtain the initial guess for the Newton's iteration in simulating the MOSFET devices [12]. As compared to the full numerical method, the analytical method takes the advantage of saving the computer resources including the CPU time and the memory space. However, it is still limited by lack of flexibility in applications for different device structures.

In this paper, a general solution method is proposed to solve the full set of 2-D semiconductor equations discretized in the finite-difference scheme. The Green's func-

Manuscript received June 17, 1991; revised January 18, 1992. This work was supported by the National Science Council, Taiwan, Republic of China under Contract NSC-78-400404-E009-26. This paper was recommended by Associate Editor D. L. Scharfetter.

The authors are with the Advanced Semiconductor Research Laboratory and the Institute of Electronics, National Chiao-Tung University, Hsinchu, Taiwan, Republic of China.

IEEE Log Number 9200920

tion in the hyperbolic-sine (hyperbolic-cosine) form [14] is adopted and discretized to calculate the 2-D potential distribution, and a surface mapping technique is developed for solving the surface potential to simulate arbitrary surface boundary conditions in the rectangular domain. Furthermore, the full set of semiconductor equations can be self-consistently solved by incorporating the proposed method with a numerical solver for the current continuity equations. The features of the proposed scheme are that: 1) the potential ripple due to Gibb's phenomenon [17], which is induced by the summation of a finite number of trigonometric series in the Green's function, can be completely eliminated, and the computation efficiency can be improved by the discretization of the Poisson's equation; 2) a surface mapping technique is used to enhance the flexibility of the discretized Green's function to treat arbitrary surface boundary conditions; 3) an SLOR-nonlinear iterative method for solving the current continuity equations is developed by using a dynamic coefficient matrix for the variation of the potential change, and the mutual coupling effect between semiconductor device equations can be properly considered. As a consequence, no outer iteration is needed for obtaining the self-consistent solution of semiconductor device equations and the required memory space is then much reduced.

In Section II, a new discretized Green's function solution method is proposed to solve the 2-D Poisson's equation and a surface mapping technique for arbitrary surface boundary conditions in the rectangular domain is described. In Section III, a new iteration scheme for the self-consistent calculation of discretized semiconductor equations is given. In order to demonstrate the usefulness of the proposed method, a Si-MESFET device operated in the high-current level is simulated, and comparisons of the performance between the proposed method and the existing method are given in Section IV. A conclusion is made in Section V.

II. A General Method for Solving the 2-D Poisson's Equation Discretized in the Finite-Difference Scheme

A. Conventional Green's Function Solution Method

The Green's function technique for semiconductor device modeling was first developed by Lin and Wu [13] in modeling the threshold voltage and the subthreshold property of short-channel MOSFET's. Comparing it to other analytical methods, the major advantage of the Green's function method is that the two-dimensional charge distribution can be exactly considered. The flexibility of the analytical method can be enhanced in treating arbitrary charge distribution by the Green's function method.

Considering the 2-D Poisson's equation in a rectangular domain shown in Fig. 1, the second-order elliptical differential equation can be written as

$$\nabla^2 \Psi(x, y) = -\frac{\rho(x, y)}{\epsilon} \tag{1}$$

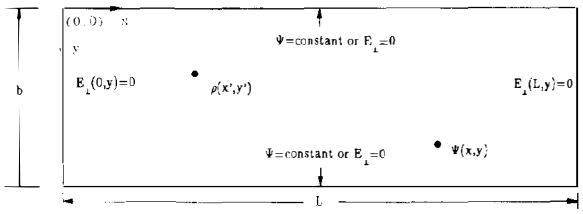

Fig. 1. The schematic cross section of a semiconductor device with the rectangular coordinate system indicated.

where $\Psi(x, y)$ is the 2-D potential distribution, $\rho(x, y)$ is the charge density distribution, and ϵ is the dielectric permittivity.

The solution of the 2-D Poisson's equation in a finite region can be obtained by means of Green's theorem [14]:

$$\Psi(x, y) = \int_{v'} G(x, y; x', y')\rho(x', y')\, dv' + \int_{s'} \epsilon \left[G(x, y; x', y') \frac{\partial \Psi}{\partial n'} - \frac{\partial G}{\partial n'} \Psi(x', y') \right] ds' \tag{2}$$

where (x, y) and (x', y') denotes the field- and source-point coordinates, respectively; $G(x, y; x', y')$ is the Green's function and must satisfy

$$\nabla'^2 G(x, y; x', y') = -\frac{1}{\epsilon} \delta(x - x')\, \delta(y - y') \tag{3}$$

where $\delta(x - x')$ and $\delta(y - y')$ are the Dirac delta functions. The Green's function $G(x, y; x', y')$ can be interpreted as the potential response of this linear operator at the field point (x, y) due to an impulse of charge introduced at the source point (x', y'). For a rectangular domain with the same dielectric permittivity, $G(x, y; x', y')$ can be expressed as a hyperbolic-sine (cosine) series of infinite terms [14]:

$$G(x, y; x', y') = \sum_m g_m(x, x') f_m(y, y') \tag{4}$$

and $g_m(x, x')$ can be expressed as

$$g_m(x, x') = A_m \sin(k_m x) \sin(k_m x') + B_m \cos(k_m x) \cos(k_m x') \tag{5}$$

where k_m is eigenvalue, A_m and B_m are the coefficients and can be determined by setting the known boundary conditions.

$f_m(y, y')$ in (4) must satisfy the following 1-D differential equation with the eigenvalue k_m:

$$\frac{d^2 f_m}{dy'^2} - k_m^2 f_m = -\frac{1}{\epsilon} \delta(y - y') \tag{6}$$

and its solution can be easily obtained as

$$f_m(y, y') = \begin{cases} \dfrac{\sinh(k_m y)\sinh k_m(b - y')}{\epsilon k_m \sinh(k_m b)}, & \text{for } y < y' \\ \dfrac{\sinh(k_m y')\sinh k_m(b - y)}{\epsilon k_m \sinh(k_m b)}, & \text{for } y > y'. \end{cases} \tag{7}$$

The number of the eigenvalue (k_m) is infinite because (1) is defined in the continuous space, and the resolution of the solution must be infinite. The following weak points will occur when (4), (5), and (7) are applied to device simulation:

1) The accuracy of simulation depends on the number of trigonometric series used. In general, the computation efficiency will degrade when the number of trigonometric series is increased. Therefore, the accuracy will be traded off with the efficiency of simulation.

2) A potential ripple will be induced by keeping a finite number of trigonometric series and will produce the unwanted current path in metal contact, as shown in Fig. 2. This effect may reduce the stability and accuracy of simulation.

3) Mixed surface boundary conditions and heterostructure devices cannot be solved by this form of Green's function.

In order to eliminate the potential ripple and improve the accuracy, a new discretized Green's function solution method is proposed to solve the 2-D Poisson's equation discretized in the finite-difference scheme. Furthermore, a surface mapping technique is developed to treat arbitrary surface boundary conditions.

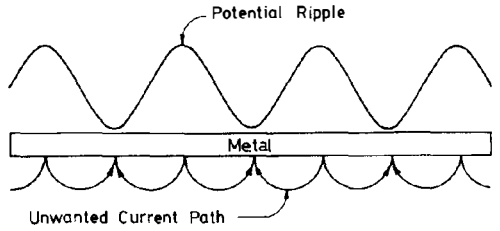

Fig. 2. An example showing the unwanted current path induced by the potential ripple.

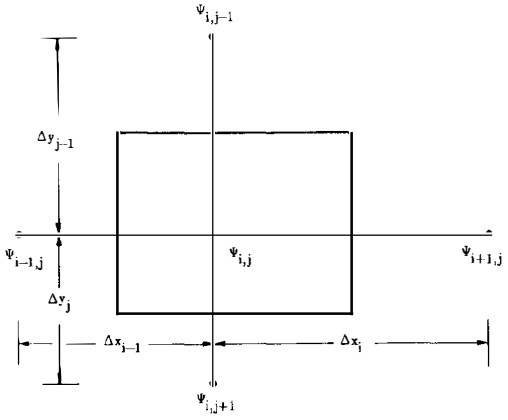

Fig. 3. The adopted nomenclature for the discretization of the 2-D Poisson's equation in the finite-difference scheme.

B. Discretized Green's Function Solution Method

According to Fig. 3, the 2-D Poisson's equation can be discretized in the finite-difference scheme as follows:

$$\frac{2}{\Delta x_i + \Delta x_{i-1}}\left(\frac{\Psi_{i+1,j} - \Psi_{i,j}}{\Delta x_i} + \frac{\Psi_{i-1,j} - \Psi_{i,j}}{\Delta x_{i-1}}\right) + \frac{2}{\Delta y_j + \Delta y_{j-1}}\left(\frac{\Psi_{i,j+1} - \Psi_{i,j}}{\Delta y_j} + \frac{\Psi_{i,j-1} - \Psi_{i,j}}{\Delta y_{j-1}}\right)$$

$$= -\frac{\rho_{i,j}}{\epsilon_j}, \qquad \text{for } 1 \le i \le i_{\max} \text{ and } 1 \le j \le j_{\max} \tag{8}$$

in which $i_{\max}$ and $j_{\max}$ are the grid number along x-direction and y-direction, respectively.

The discretized Green's function, $G(i, i'; j, j')$, is chosen to solve (8) and must satisfy

$$\frac{2}{\Delta x_{i'} + \Delta x_{i'-1}}\left(\frac{G(i, i'+1; j, j') - G(i, i'; j, j')}{\Delta x_{i'}} + \frac{G(i, i'-1; j, j') - G(i, i'; j, j')}{\Delta x_{i'-1}}\right)$$

$$+ \frac{2}{\Delta y_{j'} + \Delta y_{j'-1}}\left(\frac{G(i, i', j, j'+1) - G(i, i', j, j')}{\Delta y_{j'}} + \frac{G(i, i'; j, j'-1) - G(i, i'; j, j')}{\Delta y_{j'-1}}\right)$$

$$= \begin{cases} -\dfrac{1}{\epsilon_{j'}}\dfrac{2}{\Delta x_{i'} + \Delta x_{i'-1}}\dfrac{2}{\Delta y_{j'} + \Delta y_{j'-1}}, & \text{for } i' = i \text{ and } j' = j \\ 0, & \text{for } i' \ne i \text{ and } j' \ne j \end{cases} \tag{9}$$

Multiplying (9) with $\Psi_{i',j'}(\Delta x_{i'} + \Delta x_{i'-1})(\Delta y_{j'} + \Delta y_{j'-1})/4$ and performing the summation over all the node (i', j'). $\Psi_{i,j}$ can be obtained by substituting (8) into (9)

and is expressed as

$$\Psi_{i,j} = \epsilon_j \sum_{\substack{1<i'<i_{\max} \\ 1<j'<j_{\max}}} G(i, i'; j, j') \frac{\rho(i', j')}{\epsilon_{j'}} \frac{\Delta y_{j'} + \Delta y_{j'-1}}{2} \cdot \frac{\Delta x_{i'} + \Delta x_{i'-1}}{2} + \epsilon_j \sum_{1<j'<j_{\max}} \cdot \left(\Psi_{1,j'} \frac{G(i, 1; j, j') - G(i, 2; j, j')}{\Delta x_1} - G(i, 1; j, j') \frac{\Psi_{1,j'} - \Psi_{2,j'}}{\Delta x_1} \right) \cdot \frac{\Delta y_{j'} + \Delta y_{j'-1}}{2} + \left(\Psi_{i_{\max},j'} \frac{G(i, i_{\max}; 1, j) - G(i, i_{\max} - 1, j; j')}{\Delta x_{i_{\max}-1}} - G(i, i_{\max}; j, j') \frac{\Psi_{i_{\max},j'} - \Psi_{i_{\max}-1,j'}}{\Delta x_{i_{\max}-1}} \right) \cdot \frac{\Delta y_{j'} + \Delta y_{j'-1}}{2} + \epsilon_j \sum_{1<i'<i_{\max}} \cdot \left(\Psi_{i',1} \frac{G(i, i'; j, 1) - G(i, i'; j, 2)}{\Delta y_1} - G(i, i'; j, 1) \cdot \frac{\Psi_{i',1} - \Psi_{i',2}}{\Delta y_1} \right) \frac{\Delta x_{i'} + \Delta x_{i'-1}}{2} + \left(\Psi_{i',j_{\max}} \frac{G(i, i'; j, j_{\max}) - G(i, i'; j, j_{\max} - 1)}{\Delta y_{j_{\max}-1}} - G(i, i_{\max}; j, j') \frac{\Psi_{i',j_{\max}} - \Psi_{i',j_{\max}-1}}{\Delta y_{j_{\max}-1}} \right) \cdot \frac{\Delta x_{i'} + \Delta x_{i'-1}}{2}. \quad (10)$$

The generalized form of (10) can be derived as

$$\Psi_{i,j} = \epsilon_j \sum_{V'} G(i, i'; j, j') \frac{\rho(i', j')}{\epsilon_{j'}} \Delta V' + \epsilon_j \sum_{S'} \left(G \frac{\Delta \Psi}{\Delta n} - \frac{\Delta G}{\Delta n} \Psi \right) \Delta S' \quad (11)$$

where S' and V' denote the boundary point and the source point, respectively, and n is the outward direction in the boundary point.

It is clearly seen that (11) is the discretized Green's theorem for the 2-D Poisson's equation in the discretized domain. It is noted that the first term in the right-hand side of (11) is used to describe the potential at the field point (i, j) produced by the linear operator $G(i, j; i', j')$ for the charge density in the source point (i', j'), and the other terms exhibit the correlation between the potential distribution and the boundary conditions.

Note that the choice of a proper form for the Green's function is very important in order to decouple the potential and its potential gradient at the boundary points, as expressed in the third and second terms in the right-hand side of (11). The Green's function is set up to produce a zero potential along the boundary points for the Dirichlet boundary condition. The second term in the right-hand side of (11) vanishes due to $G(x, x'; y, y') = 0$ along the boundary points, and this means that the potential distribution can be expressed only in terms of the boundary potential and the charge distribution. Similar to the case of the Dirichlet boundary condition, the Green's function must be set up to produce a zero gradient at the boundary points for the Neumann boundary condition to decouple the relation between the potential distribution and the boundary potential. As a result of this setup, (11) can be written as

$$\Psi_{i,j} = \epsilon_j \sum_{V'} G(i, i'; j, j') \frac{\rho(i', j')}{\epsilon_{j'}} \Delta V' + \epsilon_j \sum_{N} G \frac{\Delta \Psi}{\Delta n} \Delta S' - \epsilon_j \sum_{D} \frac{\Delta G}{\Delta n} \Psi \Delta S' \quad (12)$$

where N is used to denote the Neumann boundary condition and D is used to denote the Dirichlet boundary condition.

In the rectangular domain, $G(i, i'; j, j')$ in (12) can be expressed as

$$G(i, i'; j, j') = \sum_{m} g_m(i; i') f_m(j; j') \quad (13)$$

where the Neumann boundary condition is used for the lateral sides of the simulation domain. The boundary condition at the bottom side is dependent on the device to be simulated, and the Dirichlet boundary condition is used for the surface boundary by incorporating with a surface mapping technique described in the following subsection. Furthermore, $g_m(i, i')$ in (13) can be written as

$$g_m(i; i') = g_{m,i}\, g_{m,i'} \quad (14)$$

where $g_{m,i}$ is the solution of the following linear system with the eigenvalue λ_m and the boundary condition of $\Delta g_{m,i}/\Delta x_i = 0$ for $i = 1$ and $i = i_{\max}$:

$$\frac{2}{\Delta x_i + \Delta x_{i-1}} \left(\frac{g_{m,i+1} - g_{m,i}}{\Delta x_i} + \frac{g_{m,i-1} - g_{m,i}}{\Delta x_{i-1}} \right) = \lambda_m^2 g_{m,i}, \quad \text{for } 1 < i < i_{\max}. \quad (15)$$

The linear system described in (15) is a typical eigenvalue problem. The number of the eigenvalue (λ_m) is equal to the grid number along the x-direction, and the set of the eigenvectors $(g_{m,i})$ consists of a complete mutual orthogonal set defined in the discretized points $\{x_1, x_2, \cdots, x_{i_{\max}}\}$ [15]. This means that any arbitrary function $f(x_i)$ defined in the discretized points $\{x_1, x_2, \cdots, x_{i_{\max}}\}$ can be exactly expressed as

$$f(x_i) = \sum_{m=1}^{i_{\max}} f_m g_{m,i} \quad (16)$$

where the coefficient f_m can be calculated by the following equation:

$$f_m = \sum_{i=1}^{i_{\max}} f(x_i) g_{m,i} \frac{\Delta x_i + \Delta x_{i-1}}{2} \quad (17)$$

and the eigenpair $(\lambda_m, g_{m,i})$ can be obtained by the numerical method in [16] with the defined boundary conditions.

Furthermore, incorporating with (15), $f_m(j, j')$ can be obtained by solving the following equation with the surface boundary condition of $f_m(j, 0) = 0$ and a proper bottom boundary:

$$\frac{2}{\Delta y_{j'} + \Delta y_{j'-1}}\left[\frac{f_m(j; j'+1) - f_m(j; j')}{\Delta y_{j'}} + \frac{f_m(j; j'-1) - f_m(j; j')}{\Delta y_{j'-1}}\right] - \lambda_m^2 f_m(j; j') = \begin{cases} \dfrac{-2}{\epsilon_j(\Delta y_j + \Delta y_{j-1})}, & \text{for } j' = j \\ 0, & \text{for } j' \neq j. \end{cases} \tag{18}$$

Similar to (7), (18) can be expressed as the following form:

$$f_m(j; j') = \begin{cases} u_{m,j} v_{m,j'}, & \text{for } j \leq j' \\ u_{m,j'} v_{m,j}, & \text{for } j > j' \end{cases} \tag{19}$$

where $u_{m,j}$ can be solved by substituting (19) into (18) and is given by

$$\frac{2}{\Delta y_j + \Delta y_{j-1}}\left(\frac{u_{m,j+1} - u_{m,j}}{\Delta y_j} + \frac{u_{m,j-1} - u_{m,j}}{\Delta y_{j-1}}\right) = \lambda_m^2 u_{m,j}, \quad \text{for } 1 < j < j_{\max}. \tag{20}$$

As $u_{m,j}$ is determined, $v_{m,j}$ can be obtained from the following recursive relation:

$$v_{m,j} = v_{m,j-1}\frac{u_{m,j}}{u_{m,j-1}} - \frac{\Delta y_{j-1}}{\epsilon_{j-1}}. \tag{21}$$

The potential distribution, $\Psi_{i,j}$, can be directly calculated by substituting (13), (14), and (19) into (12), and can be simplified as

$$\Psi_{i,j} = \sum_m (\tilde{U}_{m,j} v_{m,j} + \tilde{L}_{m,j} u_{m,j}) g_{m,i} \epsilon_j \tag{22}$$

where the symbol ($\sim$) is used to represent the Fourier-transformation of the eigenvector $g_{m,i}$, i.e.,

$$\tilde{X}_{m,j} = \sum_i X_{i,j} g_{m,i} \Delta x_i \tag{23}$$

and $\tilde{U}_{m,j}$ and $\tilde{L}_{m,j}$ represent the net contributions of the upper and lower planes in the field point (i, j), respectively, and can be written as

$$\tilde{U}_{m,j} = \tilde{\Psi}_{s,m} u_{m,0} + \sum_{j'<j} \frac{\tilde{\rho}_{m,j'}}{\epsilon_{j'}} u_{m,j'} \tag{24}$$

and

$$\tilde{L}_{m,j} = \tilde{\Psi}_{b,m} v_{m,j\max} + \sum_{j'\geq j} \frac{\tilde{\rho}_{m,j'}}{\epsilon_{j'}} v_{m,j'}. \tag{25}$$

Note that the potential distribution can be expressed in terms of $\tilde{\Psi}_{s,m}$, $\tilde{\Psi}_{b,m}$, and $\tilde{\rho}_{m,j}$, in which $\tilde{\Psi}_{s,m}$, $\tilde{\Psi}_{b,m}$, and $\tilde{\rho}_{m,j}$ are the Fourier transformations of the surface potential, the bottom potential, and the charge density distribution in the j'-column, respectively.

The relation between $\tilde{U}_{m,j}$ and $\tilde{U}_{m,j+1}$ can be expressed as

$$\tilde{U}_{m,j+1} = \tilde{U}_{m,j} + \frac{\tilde{\rho}_{m,j}}{\epsilon_j} u_{m,j} \tag{26}$$

and similarly, the relation between $\tilde{L}_{m,j}$ and $\tilde{L}_{m,j+1}$ can be written as

$$\tilde{L}_{m,j+1} = \tilde{L}_{m,j} - \frac{\tilde{\rho}_{m,j}}{\epsilon_j} v_{m,j}. \tag{27}$$

These two relations can be used to obtain the potential distribution efficiently when the calculation is swept from j to $j + 1$ column.

The major feature of the discretized Green's function is that the potential ripple induced by keeping a finite number of trigonometric series has been completely eliminated by the discretization of the 2-D Poisson's equation. In order to show the usefulness of (16) in eliminating the potential ripple, a step function is used as a testing example. Comparisons between a step function approximated by trigonometric series and the use of (16) are shown in Fig. 4(a). It is clearly seen that the potential ripple induced by keeping a finite number of trigonometric series is very serious; however, there occurs no potential ripple when (16) is used. Moreover, the differences between the step function and its approximations obtained by trigonometric series and (16) are plotted in a logarithmic scale, as shown in Fig. 4(b), where the residue is defined as the difference between a step function and its approximations obtained by the two specified methods. It is clearly shown that the residues of about 10 orders can be reduced as the use of the 512 terms of trigonometric series for the conventional solution method is compared to that of the 36 terms for our proposed discretized scheme in (16). Note that the residues produced by the use of (16) are mainly due to the roundoff error. Therefore, the accuracy and efficiency can be significantly improved by using the proposed discretized scheme.

C. Surface Mapping Technique

In order to calculate the potential distribution subjected to the given surface boundary conditions shown in Fig. 5, the surface potential $\tilde{\Psi}_{s,m}$ in (22) and (24) must be determined by the condition that the electric displacement at the surface is continuous across the interface. The basic concept is that the electric field produced by the charge-density distribution can be substituted by the electric field produced by the surface potential. In order to implement this effect, a transformation matrix $C_{m,m'}$ is introduced and derived as follows:

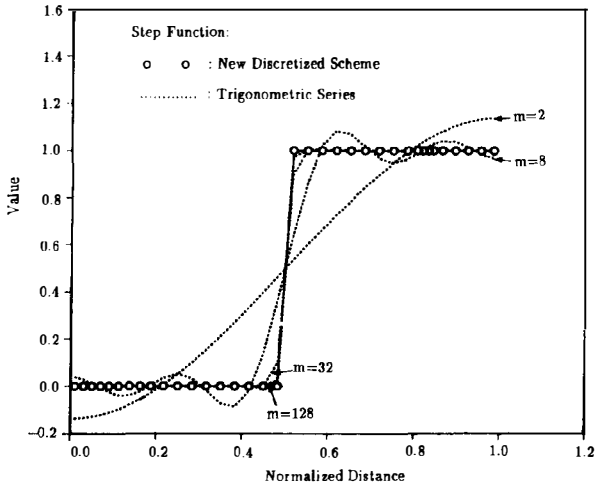

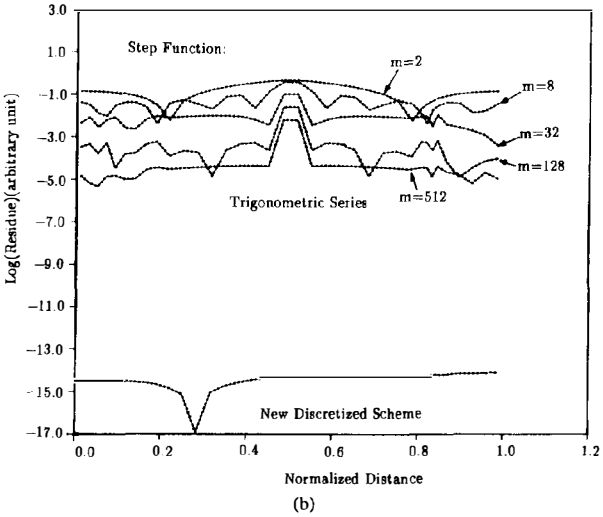

Fig. 4. (a) Comparisons of the produced potential ripple in a linear scale between two specified methods. (b) Comparisons of the residue in a logarithmic scale between two specified methods.

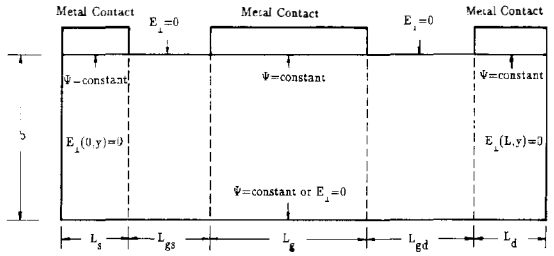

Fig. 5. An example showing the boundary conditions in a semiconductor device.

The normal electric field ($E_{1,i}$) due to the charge-density term in (22) at the surface node i can be expressed as

$$E_{1,i} = -\sum_m \epsilon_1 g_{m,i} \tilde{L}_{m,0} \left.\frac{du_m}{dy}\right|_{y=0} \tag{28}$$

and the normal electric field ($E_{2,i}$) due to the surface potential is

$$E_{2,i} = -\sum_m \epsilon_1 g_{m,i} \tilde{\Psi}_{s,m} \left.\frac{dv_m}{dy}\right|_{y=0}. \tag{29}$$

In general, the surface boundary conditions can be divided into the Neumann boundary condition(N) and the Dirichlet boundary condition(D). The function F can be defined as the continuous condition of the boundary conditions at the node i. If the node i is in the Neumann region, the normal electric field must vanish at this point:

$$F(i) = E_{1,i} + E_{2,i} = 0, \qquad \text{for } i \in N \tag{30}$$

and if the fixed surface potential is in the Dirichlet region, we obtain

$$F(i) = \sum_m \tilde{\Psi}_{s,m} g_{m,i} - \Psi^0_{s,i} = 0, \qquad \text{for } i \in D \tag{31}$$

where $\Psi^{\bullet}_{s,i}$ is the fixed surface potential. It is noted that $\Psi^0_{s,i}$ is usually denoted as the applied bias on contact metal in the node i.

Multiplying $F(i)$ by $g_{m',i}$ and performing the summation over all the node i at the surface, the following linear system can be obtained:

$$\sum_i F(i) g_{m',i} \Delta x_i = \tilde{\Psi}^0_{s,m'} + \sum_m \left(D_{m,m'} - N_{m,m'} \frac{dv_m}{dy} \right) \tilde{\Psi}_{s,m} - N_{m,m'} L_{m,0} \frac{du_m}{dy} = 0, \qquad \text{for } m' = 1, i_{\max} \tag{32}$$

where

$$D_{m,m'} = \sum_{i \in D} g_{m,i} g_{m',i} \Delta x_i, \quad N_{m,m'} = \sum_{i \in N} g_{m,i} g_{m',i} \Delta x_i$$

$$\tilde{\Psi}^0_{s,m'} = \sum_{i \in D} \Psi^0_{s,i} g_{m',i} \Delta x_i.$$

Furthermore, (32) can be rewritten in a matrix form:

$$\boldsymbol{A}\tilde{\boldsymbol{\Psi}}_s = \boldsymbol{B}\tilde{\boldsymbol{L}}_0 + \tilde{\boldsymbol{\Psi}}^0_s \tag{33}$$

where the entries of $\boldsymbol{A}$ and $\boldsymbol{B}$ are separately defined as

$$[\boldsymbol{A}]_{m,m'} = D_{m,m'} - N_{m,m} \frac{dv_m}{dy} \tag{34}$$

$$[\boldsymbol{B}]_{m,m'} = N_{m,m} \frac{du_{m'}}{dy} \tag{35}$$

and the vectors $\tilde{\boldsymbol{\Psi}}_s$, $\tilde{\boldsymbol{L}}_0$, and $\tilde{\boldsymbol{\Psi}}^0_s$ are defined as:

$$\tilde{\boldsymbol{\Psi}}_s = (\tilde{\Psi}_{s,1}, \tilde{\Psi}_{s,2}, \tilde{\Psi}_{s,3}, \cdots, \tilde{\Psi}_{s,i_{\max}})^t \tag{36}$$

$$\tilde{\boldsymbol{L}}_0 = (\tilde{L}_{1,0}, \tilde{L}_{2,0}, \tilde{L}_{3,0}, \cdots, \tilde{L}_{i_{\max},0})^t \tag{37}$$

$$\tilde{\boldsymbol{\Psi}}^0_s = (\tilde{\Psi}^0_{s,1}, \tilde{\Psi}^0_{s,2}, \tilde{\Psi}^0_{s,3}, \cdots, \tilde{\Psi}^0_{s,i_{\max}})^t. \tag{38}$$

The surface potential can be obtained by inverting a linear system of equations in (33), i.e.,

$$\tilde{\Psi}_s = \boldsymbol{C}\tilde{\boldsymbol{L}}_0 + \boldsymbol{A}^{-1}\tilde{\Psi}_s^0 \tag{39}$$

where $\boldsymbol{C} = \boldsymbol{A}^{-1}\boldsymbol{B}$, and

$$\tilde{\Psi}_{s,m} = \sum_{m'} C_{m,m'}\tilde{L}_{m',0} + A^{-1}_{m,m'}\tilde{\Psi}^0_{s,m}. \tag{40}$$

The mapping matrix $\boldsymbol{C}$ is only dependent on the device structure and the grid partition, which is fixed when the simulated structure and the grid partition are not changed during simulation. The surface potential can be directly mapped from the term $L_{m,0}$ by the mapping matrix $\boldsymbol{C}$, and the complex boundary can be solved by the proposed method. Therefore, the conventional Green's function solution method can be extended to calculate the potential distribution for the case with arbitrary surface boundary conditions in semiconductor devices. The application of this technique to a MOSFET structure can be implemented by adding a Laplace equation in the oxide region.

III. A New Iteration Scheme for Calculating the Discretized Semiconductor Device Equations

In order to develop a general-purpose device simulator with the capability of simulating various device structures including heterostructures with arbitrary surface boundaries in the rectangular domain and operated under any operation bias condition, the full set of semiconductor device equations including the Poisson's equation and the continuity equations of both carriers must be solved self-consistently. In this section, a new iterative scheme for solving these equations simultaneously is developed by incorporating the discretized Green's function solution with the SLOR method.

The discretization of current continuity equations is based on the finite-difference scheme originally proposed by Schafetter and Gummel [9], and later extended to the multidimensional case by using the box-method. The current continuity equations of both carriers can be discretized at the node (i, j). For electron current continuity equation, we obtain

$$E^0_{i,j}n_{i,j} + E^1_{i,j}n_{i,j-1} + E^2_{i,j}n_{i-1,j} + E^3_{i,j}n_{i,j+1} + E^4_{i,j}n_{i+1,j} = G^n_{i,j} \tag{41}$$

and for hole current continuity equation, we obtain

$$H^0_{i,j}p_{i,j} + H^1_{i,j}p_{i,j-1} + H^2_{i,j}p_{i-1,j} + H^3_{i,j}p_{i,j+1} + H^4_{i,j}p_{i+1,j} = G^p_{i,j} \tag{42}$$

where the content of each term in (41) and (42) can refer to [8].

The discretized equations described in (41) and (42) form a linear system with n and p as the variables, and also form a nonlinear system in terms of the potential distribution. Since the potential distribution is a function of the charge-density distribution, (41) and (42) form implicitly the nonlinear systems for carrier densities (n and p). Therefore, the weak points of using the conventional numerical methods are obvious and described as follows.

1) The linear expansions of (41) and (42) are not valid when the potential change is too large. The Newton's method, which is based on this technique to describe the mutual coupling effect between these equations, will diverge if the initial guess for the Newton's iteration is not good enough to keep the linear expansions of (41) and (42) valid.

2) The mutual coupling effect is not properly considered in the Gummel's method. The Gummel's method will exhibit slow convergence if the mutual coupling effect between these equations is strong.

A new algorithm, which incorporates the Poisson's solver with the current continuity equation solver, is developed to properly model the mutual coupling effect. The basic concept is that the potential distribution for the precalculated charge can be obtained from (22) and (40), and the coefficient matrix for the current continuity equations can be updated by the dynamic response to the change of the potential when performing the numerical SLOR iteration to solve (41) and (42). The potential can be treated as a linear response to the charge-density distribution by the discretized Green's function solution method developed in Section II. A modified SLOR method is used to implement the proposed new algorithm.

The proposed algorithm is somewhat similar to the standard SLOR method. However, the coefficient matrix for the current continuity equations is modified to dynamically response to the change of the potential distribution directly calculated from the discretized Green's function solution method in Sections II-B and II-C. Therefore, the proposed algorithm is different from the standard SLOR method with a fixed coefficient matrix. The algorithm is explained as follows:

Step 1: From (41) and (42), the potential distributions involved to describe the current continuity equation in the j-column are $j-1$, j, $j+1$. The potential distributions in these columns can be generated by (22) and (40), i.e.,

$$\Psi^k_{i,j-1} = \sum_m (\tilde{U}^k_{m,j-1}v_{m,j-1} + \tilde{L}^k_{m,j-1}u_{m,j-1})g_{m,i}\epsilon_{j-1} \tag{43}$$

$$\Psi^k_{i,j} = \sum_m (\tilde{U}^k_{m,j}v_{m,j} + \tilde{L}^k_{m,j}u_{m,j})g_{m,i}\epsilon_j \tag{44}$$

$$\Psi^k_{i,j+1} = \sum_m (\tilde{U}^k_{m,j+1}v_{m,j+1} + \tilde{L}^k_{m,j+1}u_{m,j+1})g_{m,i}\epsilon_{j+1} \tag{45}$$

where the superscript k denotes the kth iteration.

Step 2: The coefficient matrix for the current continuity equations at the node point in the jth column is calculated by (41) and (42).

Step 3: The carrier density at the node point in the jth column is obtained from solving the system of linear equations by using the $j+1$ and $j-1$ columns as the boundary conditions. The matrix form denotes that this

iteration can be written with a relaxation factor ω as

$$\boldsymbol{n}_j^{c,k} = (1 - \omega)\boldsymbol{n}_j^{k-1} + \omega[\boldsymbol{B}_{n,j}^k]^{-1} \cdot (\boldsymbol{G}_j^{n,k} - \boldsymbol{A}_{n,j}^k \boldsymbol{n}_{j-1}^k - \boldsymbol{C}_{n,j}^k \boldsymbol{n}_{j+1}^{k-1}) \quad (46)$$

where the vectors $\boldsymbol{n}_j^{c,k}$ and $\boldsymbol{G}_j^k$ are the electron density calculated from current continuity equation and the electron generation-rate in the j-column at the kth iteration, respectively, and can be written as

$$\boldsymbol{n}_j^{c,k} = (n_{1,j}^{c,k}, n_{2,j}^{c,k}, n_{3,j}^{c,k}, \cdots, n_{i\max,j}^{c,k})^t \quad (47)$$

$$G_j^{n,k} = (G_{1,j}^{n,k}, G_{2,j}^{n,k}, G_{3,j}^{n,k}, \cdots, G_{i\max,j}^{n,k})^t \quad (48)$$

the vector $\boldsymbol{n}_j^k$ represents the electron density in the j-column at the kth iteration, which is obtained from $\boldsymbol{n}_j^{c,k}$ as described in Step 4 and is written as

$$\boldsymbol{n}_j^k = (n_{1,j}^k, n_{2,j}^k, n_{3,j}^k, \cdots, n_{i\max,j}^k)^t \quad (49)$$

and the matrices $\boldsymbol{A}_{n,j}^k$, $\boldsymbol{B}_{n,j}^k$, and $\boldsymbol{C}_{n,j}^k$ can be expressed as

$$\boldsymbol{A}_{n,j}^k = \begin{bmatrix} E_{1,j}^{1,k} & & & \\ & E_{2,j}^{1,k} & & \\ & & E_{3,j}^{1,k} & \\ & & & E_{i\max,j}^{1,k} \end{bmatrix} \quad (50)$$

$$\boldsymbol{B}_{n,j}^k = \begin{bmatrix} E_{1,j}^{0,k} & E_{1,j}^{4,k} & & & \\ E_{2,j}^{2,k} & E_{2,j}^{0,k} & E_{2,j}^{4,k} & & \\ & E_{3,j}^{2,k} & E_{3,j}^{0,k} & E_{3,j}^{4,k} & \\ & & & E_{i\max,j}^{2,k} & E_{i\max,j}^{0,k} \end{bmatrix} \quad (51)$$

and

$$\boldsymbol{C}_{n,j}^k = \begin{bmatrix} E_{1,j}^{3,k} & & & \\ & E_{2,j}^{3,k} & & \\ & & E_{3,j}^{3,k} & \\ & & & E_{i\max,j}^{3,k} \end{bmatrix}. \quad (52)$$

The similar treatment can be performed for the hole continuity equation and is denoted by

$$\boldsymbol{p}_j^{c,k} = (1 - \omega)\boldsymbol{p}_j^{k-1} + \omega[\boldsymbol{B}_{p,j}^k]^{-1} \cdot (\boldsymbol{G}_j^{p,k} - \boldsymbol{A}_{p,j}^k \boldsymbol{p}_{j-1}^k - \boldsymbol{C}_{p,j}^k \boldsymbol{p}_{j+1}^{k-1}). \quad (53)$$

Step 4: It is noted that when the carrier densities are calculated by Step 3, the potential change due to the change of charge density is not considered in this column, and the change of carrier densities calculated from Step 3 will be overestimated. However, the damping method as described in the Appendix is adopted to prevent the overshoot. The changes of carrier densities in the j-column ($\Delta n_{i,j}^k$ and $\Delta p_{i,j}^k$) obtained by using the damping method are updated for the current continuity equations and the Poisson's equation, i.e.,

$$n_{i,j}^k = n_{i,j}^{k-1} + \Delta n_{i,j}^k \quad (54)$$

$$p_{i,j}^k = p_{i,j}^{k-1} + \Delta p_{i,j}^k \quad (55)$$

and

$$\rho_{i,j}^k = \rho_{i,j}^{k-1} + \Delta p_{i,j}^k - \Delta n_{i,j}^k. \quad (56)$$

The potential distributions in the j, $j + 1$, $j + 2$ columns are calculated from the discretized Green's function solution method, and the iteration is performed for the $j + 1$ column. The iteration is continued until the stopping criterion is reached.

The algorithm for the SLOR-nonlinear iteration can be summarized as follows:

Procedure SLOR-nonlinear_iteration
  For k from 1 to kmax **do**
    For j from 1 to jmax **do**
      For i from 1 to imax **do**
        Calculate $\Psi_{i,j-1}^k$, $\Psi_{i,j}^k$ and $\Psi_{i,j+1}^k$
      End for
      Calculate $\boldsymbol{G}_j^{n,k}$, $\boldsymbol{B}_{n,j}^k$, $\boldsymbol{A}_{n,j}^k$, $\boldsymbol{C}_{n,j}^k$, $\boldsymbol{G}_j^{p,k}$, $\boldsymbol{B}_{p,j}^k$, $\boldsymbol{A}_{p,j}^k$, and $\boldsymbol{C}_{p,j}^k$
      Solve $\boldsymbol{n}_j^{c,k}$ and $\boldsymbol{p}_j^{c,k}$
      Get $\Delta\boldsymbol{n}_j^k$ and $\Delta\boldsymbol{p}_j^k$ from $\boldsymbol{n}_j^{c,k}$ and $\boldsymbol{p}_j^{c,k}$ by damping method, respectively.
      Update the variables for carrier continuity equations
        $\boldsymbol{n}_j^k = \boldsymbol{n}_j^{k-1} + \Delta\boldsymbol{n}_j^k$
        $\boldsymbol{p}_j^k = \boldsymbol{p}_j^{k-1} + \Delta\boldsymbol{p}_j^k$
      Update the charge-density distribution for Poisson's equation
        $\rho_j^k = \rho_j^{k-1} + \Delta\boldsymbol{p}_j^k - \Delta\boldsymbol{n}_j^k$
    End for
    if the stopping criterion is reached **then**
      stop
    End if
  End for
End SLOR-nonlinear_iteration

The matrix form of the conventional SLOR iteration method, which needs another outer iteration to get the self-consistent solution, can be expressed as

$$\boldsymbol{n}_j^{l,k} = (1 - \omega)\boldsymbol{n}_j^{l,k} + \omega[\boldsymbol{B}_{n,j}^l]^{-1} \cdot (\boldsymbol{G}_j^{n,l,k} - \boldsymbol{A}_{n,j}^l \boldsymbol{n}_{j-1}^{l,k} - \boldsymbol{C}_{n,j}^l \boldsymbol{n}_{j+1}^{l,k-1}) \quad (57)$$

and

$$\boldsymbol{p}_j^{l,k} = (1 - \omega)\boldsymbol{p}_j^{l,k} + \omega[\boldsymbol{B}_{p,j}^l]^{-1} \cdot (\boldsymbol{G}_j^{p,l,k} - \boldsymbol{A}_{p,j}^l \boldsymbol{p}_{j-1}^{l,k} - \boldsymbol{C}_{p,j}^l \boldsymbol{p}_{j+1}^{l,k-1}) \quad (58)$$

where the symbol l denotes the lth outer iteration. Note that the equations needed to be solved are the current con-

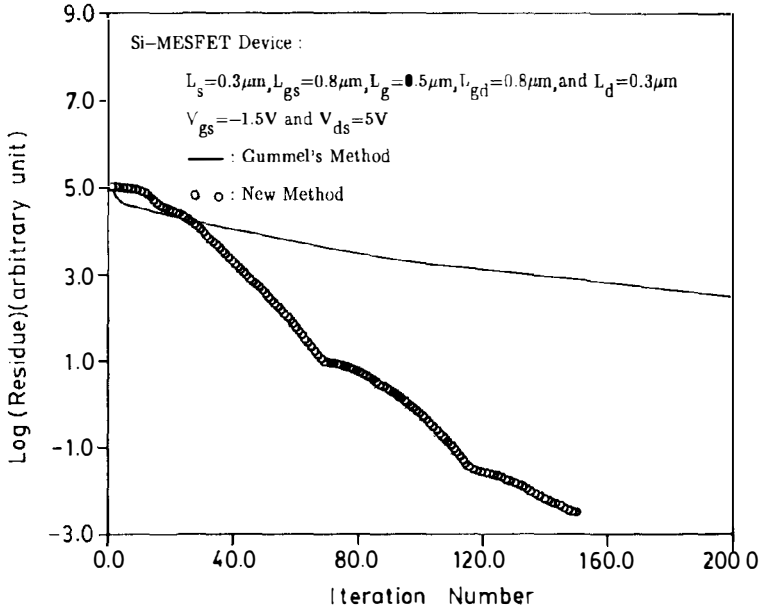

Fig. 6. Comparisons of the convergent rate between the Gummel's method and the proposed method with V_{ds} = 5 V and V_{gs} = −1.5 V.

tinuity equations of both carriers in (41) and (42) and the variables chosen for iteration are (n, p) because the potential distribution can be obtained from (22) and (40) exactly. The coefficient matrix for the current continuity equation can be changed due to the change of the potential during simulation, and the full set of semiconductor equations is solved simultaneously by the SLOR iteration. The major difference between the proposed method and the standard SLOR method is that the other outer iteration is needed for the standard SLOR method to obtain the self-consistent solution of semiconductor equations. This outer iteration may cause another convergent problem.

It is noted that the memory space needed to perform this iteration is proportional to ($3 \times i_{max}$) because the coefficient matrix is updated for each column in every iteration. The convergent property of the proposed method is limited by the intrinsic convergent property of the SLOR method and is sensitive to the relaxation factor (ω). However, the convergent rate becomes poor in some cases because the SLOR method does not converge efficiently. This drawback can be improved by using a direct method for solving the matrices obtained by the discretized current continuity equations.

IV. Results and Discussions

The use of the Newton's method for semiconductor device simulation is limited by the requirement of a proper choice of the initial guess and cannot converge if the initial guess is not in the contraction domain. In general, the Newton's method needs a solution method insensitive to the initial guess to improve the quality of the initial guess before switching to the Newton's method. Therefore, the Gummel's method is chosen to compare with the proposed method because the initial guess strategy is not necessary for the Gummel's method.

The Si-MESFET device with the floating substrate is used as a test example. This device can be operated as FET or diode mode, depending on the bias condition. The device structure is illustrated in Fig. 4 with L_S = 0.3 μm, L_{gs} = 0.8 μm, L_g = 0.5 μm, L_{gd} = 0.8 μm, L_d = 0.3 μm, and $N_d = 2 \times 10^{17}/\text{cm}^3$. It is noted that the floating substrate is assumed for the substrate boundary condition, i.e., $E_\perp = 0$ for $y = b$. The grid points used are 56 × 20 (lateral grid points × vertical grid points). The Si-film thickness is 0.2 μm, in which the grid spacing is 100 Å. The pinchoff voltage is about 6 V, and the mobility model and its parameters used are the same as those used in [13].

In order to make a clear comparison between different algorithms. The residue at the kth iteration (R_k) for different algorithms is defined as the difference between the carrier densities at the kth iteration ($n_{i,j}^k$ and $p_{i,j}^{c,k}$), and the carrier densities solved from the current continuity equations ($n_{i,j}^{c,k}$ and $p_{i,j}^{c,k}$), and can be described in the following algorithm:

Procedure obtain_residue
  For j from 1 to j_{max} **do**
    For i from 1 to imax **do**

$$\rho_{i,j}^k = N_d + p_{i,j}^k - n_{i,j}^k$$

    End for
  End for
  Calculate $\Psi_{i,j}^k$ for each node point (i, j)
  Calculate $n_{i,j}^{c,k}$ and $p_{i,j}^{c,k}$ from current continuity equations
  $R_k = 0$
  For j from 1 to j_{max} **do**

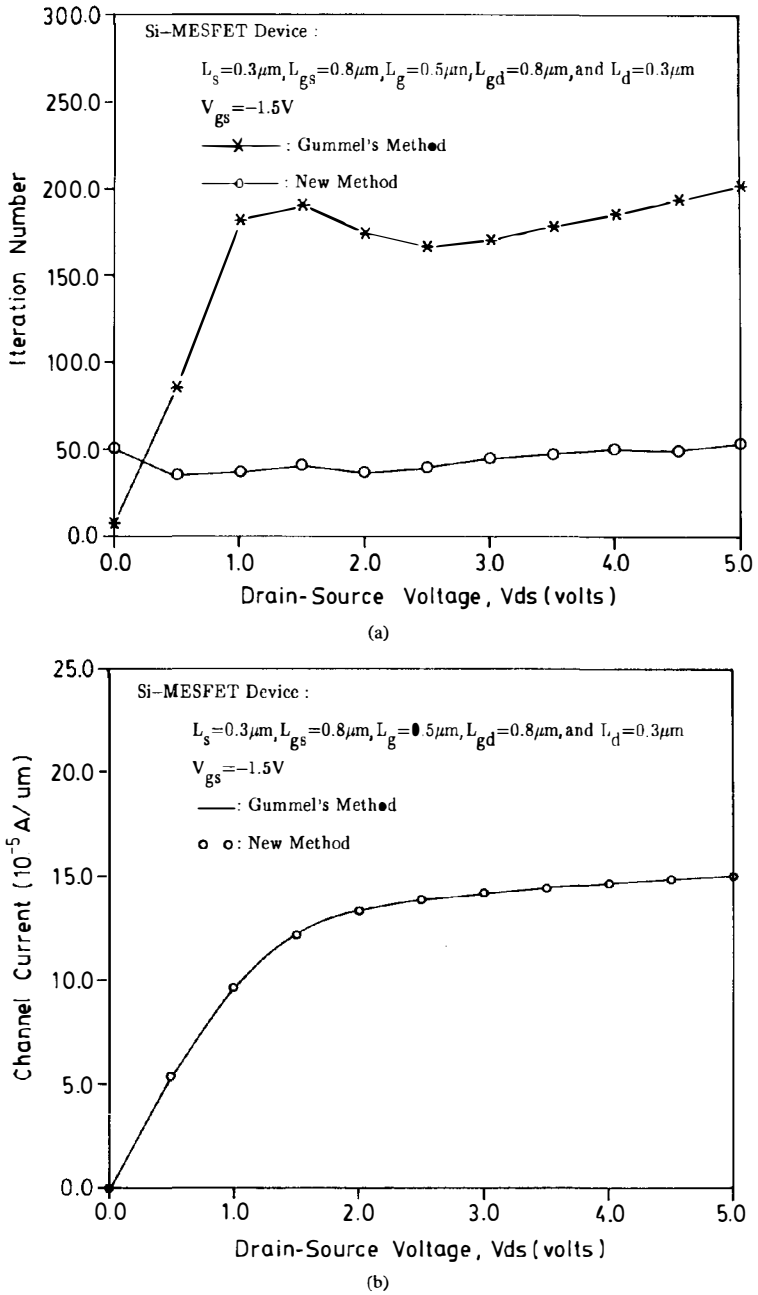

Fig. 7. Comparisons between the Gummel's method and the proposed method for continuous simulation with V_{ds} = 0–5 V and V_{gs} = −1.5 V. (a) iteration number and (b) I–V characteristic.

For i from 1 to i_{max} **do**

$$R_k = R_k + |n_{i,j}^{c,k} - n_{i,j}^k| + |p_{i,j}^{c,k} - p_{i,j}^k|$$

End for
End for
End obtain_residue

Note that the potential is calculated from the precalculated charge density ($\rho_{i,j}^k$), and the carrier densities are solved from the current continuity equations by using the direct method for the potential distribution at the kth iteration ($\Psi_{i,j}^k$).

Fig. 6 shows a comparison of the convergent rate between the proposed method and the Gummel's method. The device is biased at V_{ds} = 5 V and V_{gs} = −1.5 V, and the initial condition is set to be in the quasi-neutrality condition, i.e., $n = N_d$ and $p = n_i^2/n$. It is noted from Fig. 6 that the convergent rate of the proposed method is 4 times faster than that of the Gummel's method. Fig. 7(a)

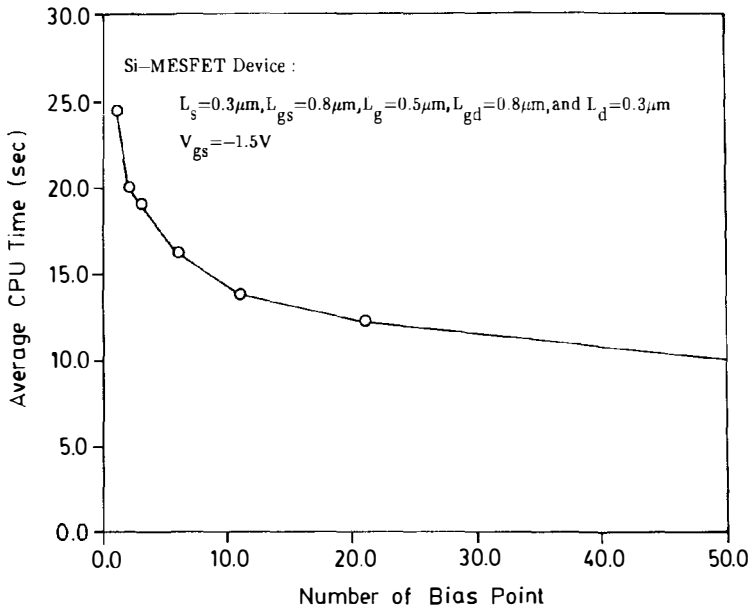

Fig. 8. The average CPU time versus bias points for continuous simulation with V_{ds} = 0–5 V and V_{gs} = 1.5 V.

shows a comparison of the iteration number versus different biases for continuous simulation, and the simulated I–V characteristic is shown in Fig. 7(b). From Fig. 7(a), the iteration number of a proposed method is less than that of the Gummel's method by a factor 4 for a given stopping criterion.

The simulation speed is proportional to the convergent rate and the CPU time per iteration. However, the CPU time per iteration for the Gummel's method strongly depends on the matrix solver and the nonlinear iteration method used. The average CPU time run by a IBM RS/6000 workstation versus bias points for continuous simulation is shown in Fig. 8. From this figure, it is known that the proposed method is insensitive to the initial condition used.

In order to show the stability of the proposed method, the simulation is performed with the drain bias of 100 V and under the initial condition of quasi-neutrality, and the result is shown in Fig. 9. From this figure, the limitation of the bias step does not exist in our proposed method.

A hybrid method, which combines the proposed method and the Gummel's method, is used to simulate the diode mode of the device. The Schottky diode is turned on when the gate bias is V_{gs} = 1.5 V. The convergent rate of the hybrid method is shown in Fig. 10, in which the residue of 12 orders is reduced within about 100 iterations. The convergent rate is much larger than the Gummel's method but is less than the Newton's method. However, the Newton's method shows two major disadvantages: one is that a great computation effort is required to solve a large linear system derived from the discretization of semiconductor device equations; the other is that the initial guess must be within the contraction domain and the additional method is needed to improve the quality of the initial guess such as the Gummel's method or the analytic model [12].

The convergent rate of the standard SLOR method is strongly dependent on the relaxation factor (ω), and the speed of the convergent rate should trade off with the stability. The convergent rate can be speeded up by using a large relaxation factor but the stability becomes worse. The convergent property versus the SLOR iteration is shown in Fig. 11. It is shown that the convergent property keeps the same as the standard SLOR method. The relaxation factor can be optimized to speed up the convergent rate in the stable scheme. It is found that the simulation will diverge when the chosen relaxation factor is greater than 1.3.

It is interesting to note that the proposed new methodology can be extended to the case of a nonplanar device structure by a new Fourier-conformal mapping method which will be addressed in our future publications.

V. Conclusion

A new methodology for 2-D numerical simulation of semiconductor devices has been proposed, in which the 2-D potential distribution is derived by a new discretized Green's function solution method in the rectangular domain. The flexibility of the proposed solution method can be further improved by a surface mapping technique to treat arbitrary surface boundary conditions. In addition, the full set of semiconductor equations can be solved by a new SLOR-nonlinear iteration technique in which the

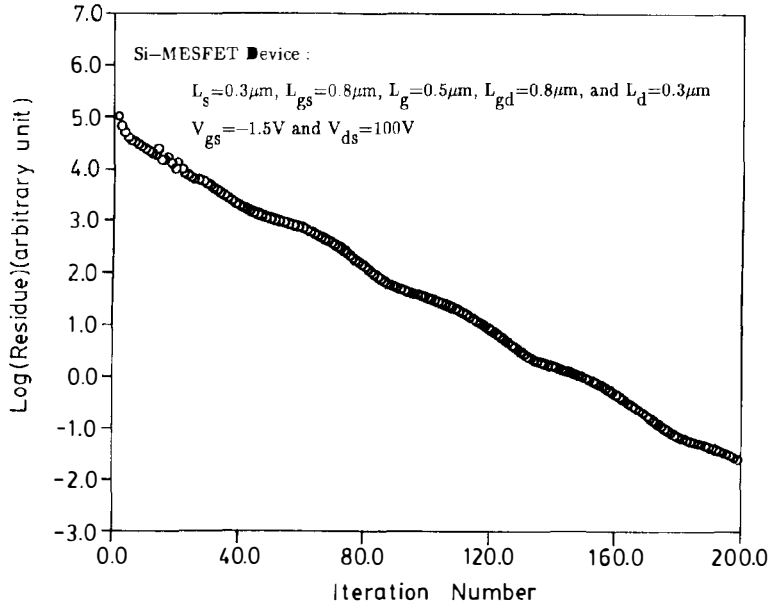

Fig. 9. The convergent rate of the proposed method for V_{ds} = 100 V and V_{gs} = −1.5 V.

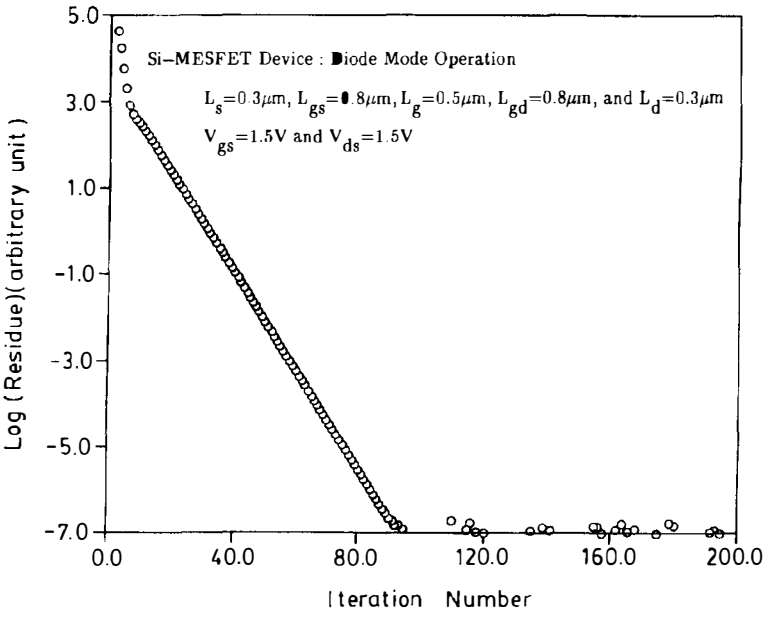

Fig. 10. The convergent rate of the hybrid method for the device operated in the diode mode with V_{ds} = 1 V and V_{gs} = 1.5 V

matrix element can be updated for the potential change due to the linear response to the change of the charge density. The proposed new methodology has been implemented in Fortran code and run at an IBM RS/6000 workstation. It has been shown that the use of the discretized Green's function solution method in semiconductor device simulation is extremely practical from the tested example. Moreover, the convergent property of the Gummel's method can be significantly improved by the proposed new method.

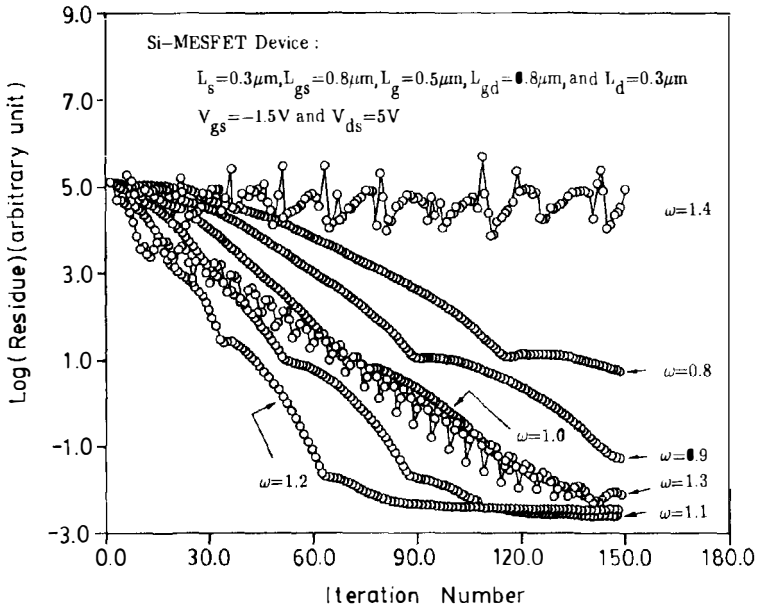

Fig. 11. Comparisons of the convergent rate for different relaxation factors (ω) with V_{ds} = 5 V and V_{gs} = −1.5 V.

Appendix

The Damping Method

The carrier density can be expressed in terms of the quasi-Fermi level as:

$$n_{i,j}^{c,k} = n_i \exp\left[\frac{q}{k_b T}(\Psi_{i,j}^{k} - \varphi_{i,j}^{n,k})\right] \tag{A1}$$

where $\Psi_{i,j}^{k}$ and $\varphi_{i,j}^{n,k}$ are the electrostatic potential and the quasi-Fermi potential for electrons in the node (i, j) at the kth iteration, respectively.

At the kth iteration, (A1) can be rewritten in the following form when the potential is changed with changing the carrier density:

$$n_{i,j}^{k-1} + \Delta n_{i,j}^{k} = n_i \exp\left[\frac{q}{k_b T}(\Psi_{i,j}^{k} - \varphi_{i,j}^{n,k} + \Delta\Psi_{i,j})\right]$$

$$= n_{i,j}^{c,k} \exp\left(\frac{q}{k_b T}\Delta\Psi_{i,j}\right). \tag{A2}$$

The potential change in the node (i, j), $\Delta\Psi_{i,j}$, which is induced by the change of carrier density in the column j, can be roughly estimated by the superposition principle:

$$\Delta\Psi_{i,j} = W_{i,j}\Delta n_{i,j}^{k} \tag{A3}$$

where $W_{i,j}$ is a proportional constant in the node (i, j) and can be calculated from (20) and (38).

Substituting (A3) into (A2), we obtain

$$n_{i,j}^{k-1} + \Delta n_{i,j}^{k} = n_{i,j}^{c,k} \exp\left(\frac{q}{k_b T} W_{i,j}\Delta n_{i,j}^{k}\right). \tag{A4}$$

The change of carrier density at the iteration k ($\Delta n_{i,j}^{k}$) is less than $n_{i,j}^{c,k} - n_{i,j}^{k-1}$ by a factor $\exp((q/k_b T)\, W_{i,j}\Delta n_{i,j}^{k})$ from (A4), and can be obtained by solving (A4) in terms of carrier density as

$$\Delta n_{i,j}^{k} = \frac{1}{W_{i,j}} \ln\left\{1 + \frac{n_{i,j}^{c,k}}{n_{i,j}^{k-1}} \cdot \left[\exp\left(-\frac{q}{k_b T} W_{i,j} n_{i,j}^{k-1}\right) - 1\right]\right\}. \tag{A5}$$

Similarly, the equivalent equation for holes can be obtained.

Acknowledgment

The authors would like to express their sincere thanks to R.-K. Perng for his helpful discussions.

References

[1] R. R. Troutman, "VLSI limitation from drain-induced barrier lowering," *IEEE Trans. Electron Devices*, vol. ED-26, pp. 461-468, 1979.

[2] M. R. Pinto, C. S. Rafferty, and R. W. Dutton, "PISCES-II Poisson and continuity equation solver," Stanford Electronics Lab. Rep., 1984.

[3] G. Baccarani, R. Guerrieri, P. Ciampolini, and M. Rudan, "HFIELDS: A highly-flexible 2-D semiconductor devices analysis program," in *Proc. NASECODE IV Conf.*, 1985, pp. 3-12.

[4] S. Selberherr, A. Schutz, and H. W. Potzl, "MINIMOS—A two-dimensional MOS transistor analyzer," *IEEE Trans. Electron Devices*, vol. ED-27, pp. 1540-1549, 1980.

[5] G. L. Tan, X. L. Yuan, Q. M. Zhang, W. H. Ku, and A. J. Shey, "Two-dimensional semiconductor device analysis based on new finite-element discretization employing the S-G scheme," *IEEE Trans. Computer-Aided Design*, vol. 8, pp. 468-478, May 1989.

[6] R. E. Bank, D. J. Rose, and W. Fichtner, "Numerical methods for semiconductor device simulation," *IEEE Trans. Electron Devices*, vol. ED-30, pp. 1031–1041, 1983.
[7] H. K. Gummel, "A self-consistent iterative scheme for one-dimensional steady state transistor calculations," *IEEE Trans. Electron Devices*, vol. ED-11, pp. 455–465, 1964.
[8] S. Selberherr, *Analysis and Simulation of Semiconductor Devices*. Vienna, Austria: Springer-Verlag, 1984.
[9] D. Scharfetter and H. K. Gummel, "Large signal analysis of silicon Read diode oscillator," *IEEE Trans. Electron Devices*, vol. ED-16, pp. 64–77, 1969.
[10] C. S. Rafferty, M. R. Pinto, and R. W. Dutton, "Iterative methods in semiconductor device simulation," *IEEE Trans. Electron Devices*, vol. ED-32, pp. 2018–2027, 1985.
[11] V. Axelrad, "Fourier method modeling of semiconductor devices," *IEEE Trans. Computer-Aided Design*, vol. 9, pp. 1225–1239, Nov. 1990.
[12] R. K. Perng, P. S. Lin, and C. Y. Wu, "A new methodology for developing a fast two-dimensional MOSFET device simulator," *Solid-State Electron.*, vol. 34, no. 6, pp. 635–648, 1991.
[13] P. S. Lin and C. Y. Wu, "A new approach to analytically solving the two-dimensional Poisson's equation and its application in short-channel MOSFET modeling," *IEEE Trans. Electron Devices*, vol. ED-34, pp. 1947–1956, 1987.
[14] J. D. Jackson, *Classical Electrodynamics*. New York: Wiley, 1975.
[15] I. Satake, *Linear Algebra*. New York: Markel-Dekker, 1975.
[16] C. F. Gerald and P. O. Wheatley, *Applied Numerical Analysis*. Reading, MA: Addison-Wesley, 1984.
[17] P. M. Morse and H. Feshback, *Methods of Theoretical Physics*. New York: McGraw-Hill, 1975.

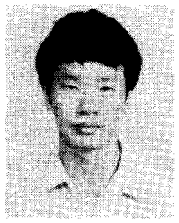

Shan-Ping Chin (S'86) was born in Taiwan, Republic of China, on September 21, 1961. He received the B.S. degree in physics from the National Tsing-Hua University, Taiwan, Republic of China, in 1985, and the M.S. degree from the Institute of Electronics, National Chiao-Tung University. He is currently working toward the Ph.D. degree and engages in device physics and new simulation techniques for deep-submicrometer MESFET's in the Advanced Semiconductor Device Research Laboratory.

Chin-Yuan Wu (M'72) was born in Taiwan, Republic of China, on March 18, 1946. He received the B.S. degree in electrical engineering from the National Taiwan University, Taiwan, Republic of China, in 1968, and the M.S. and Ph.D. degrees from the State University of New York (SUNY) at Stony Brook, in 1970 and 1972, respectively.

During the 1972–1973 academic year, he was appointed Lecturer at the Department of Electrical Sciences, SUNY, Stony Brook. From 1973–1975 he was a Visiting Associate Professor at National Chiao-Tung University (NCTU), Taiwan. In 1976, he became a Full Professor in the Department of Electronics and the Institute of Electronics. In NCTU, he had been the Director of Engineering Laboratories and Semiconductor Research Center during 1974–1980; the Director of the Institute of Electronics during 1978–1984; and the Dean, College of Engineering, during 1984–1990. He was a principal investigator of the National Electronics Mass Plan—Semiconductor Devices and Integrated-Circuit Technologies, during 1976–1979, and had been a Coordinator of the National Microelectronics Researches and High-Level Man-Power Education Committee, National Science Council, Republic of China, during 1982–1988. He has been the Research Consultant of the Electronics Research and Service Organization (ERSO), ITRI; a member of the Academic Review Committee, the Ministry of Education; and the chairman of the Technical Review Committee on Information and Microelectronics Technologies, the Ministry of Economic Affairs. His research activities have been in semiconductor device physics and modelings, integrated circuit designs and technologies. His present research areas focus on the developments of efficient 2D and 3D simulators for deep-submicrometer semiconductor devices, design rules and optimization techniques for deep-submicrometer CMOS devices, and key technologies for deep-submicrometer CMOS devices. He has published over 150 papers in the semiconductor field and has served as a reviewer for international journals such as IEEE ELECTRON DEVICE LETTERS, IEEE TRANS. ON ELECTRON DEVICES, SOLID-STATE ELECTRONICS, etc.

Dr. Wu is a member of the Honorary Editorial Advisory Board of Solid-State Electronics and is a board member of the Chinese Engineering Society. He received the Academic Research Award in Engineering from the Ministry of Education (MOE), in 1979; the outstanding Scholar award from the Chinese Educational and Cultural Foundation in 1985. He has received the outstanding Research Professor fellowship from the Ministry of Education and the National Science Council (NSC), Republic of China, during 1982–1991.